Electronic Supplementary Material (ESI) for CrystEngComm.

Electronic Supplementary Information

Cyclodextrins: a New and Effective Class of Co-Modulators for Aqueous Zirconium-MOF Syntheses

Guillaume Hoyez,[a] Jolanta Rousseau,[a] Cyril Rousseau,[a] Sébastien Saitzek,[a] James King,[b] Petra Agota Szilagyi,[b] Christophe Volkringer,[c] Thierry Loiseau,[c] Frédéric Hapiot,[a] Eric Monflier,[a] and Anne Ponchel,[a,*]

a. Univ. Artois, CNRS, Centrale Lille, Univ. Lille, UMR 8181 – UCCS – Unité de Catalyse et Chimie du Solide, F-62300 Lens, France.

b. Queen Mary University of London, School of Engineering and Materials Science, Mile End Road, E1 4NS London, UK.

c. Univ. Lille, CNRS, Centrale Lille, Univ. Artois, UMR 8181 – UCCS – Unité de Catalyse et Chimie du Solide, F-59000 Lille, France.

Materials and methods

Chemicals

All solvents and reagents were purchased from commercial vendors and used as received. Zirconium (IV) oxychloride octahydrate ($ZrOCl_2 \cdot 8H_2O$, 99,5%), *N,N*-dimethylformamide (DMF, 99,8%) were purchased from Sigma Aldrich, Germany and USA. 2-aminoterephthalic acid ($H_2BDC\text{-}NH_2$, 99%) was bought from Acros Organics, New Jersey, USA - Strem Chemicals, USA; acetic acid (CH_3COOH, 99,7%) – Fisher Scientific; methanol (CH_3OH, 99,9%) - Verbiese, France; ethanol (C_2H_5OH, 99%).

Grinding under ball-milling conditions

The experiments were conducted using a laboratory-scale ball-mill (Retsch MM400) equipped with 10 mL zirconia grinding jars containing a zirconia ball (9 mm ⌀). The grinding jars were horizontally shaken at an oscillation frequency of 30 Hz (frequency of the rocking back-and-forth motion conducted by the reaction jar holder).

Fourier-transform infrared spectroscopy (FTIR)

Infrared experiments were performed using a Spectrum two Elmer FT-IR spectrometer equipped with a single-reflection diamond module (ATR) and a deuterated triglycine sulfate detector (DGTS) (MCT) detector. FTIR spectra were recorded in the 400−4000 cm^{-1} wavenumber range with a 1 cm^{-1} resolution.

Diffraction

X-Ray Diffraction (XRD) measurements were performed using a Rigaku ULTIMA IV diffractometer equipped with Cu anticathode (λK_α = 1.5418 Å), Soller slits to limit the divergence of X-ray beam and a nickel foil filter attenuates the Cu K_β line. XRD patterns were recorded in the range of 3°-50° (scan speed of 0. 400°.min^{-1}) using the Bragg-Brentano configuration. The average crystallite size was determined using Scherrer's relation[1] by deconvoluting the instrumental part in the Full Width at Half Maximum (FWHM).

Thermogravimetric measurements (TGA) and differential Scanning Calorimetry (DSC)

TG analysis was performed using a Mettler Toledo TGA/DSC 3+ Start System instrument equipped with a flow gas system. The solid was treated from 40 °C to 1000 °C (5 °C.min^{-1}) under air (50 mL.min^{-1}).

Nitrogen Adsorption–Desorption

N_2 sorption isotherms were collected at -196 °C using an adsorption analyzer Micromeritics Tristar II 3020. Prior to analysis, 80 – 100 mg of a freshly dried sample (100 °C, overnight) was degassed for 2 hours at 100 °C under vacuum. For the surface areas estimation, Langmuir and Brunauer-Emmett-Teller (BET) models were applied to fit the experimental data.

[1] A. Patterson, *Phys. Rev.* **1939**, *56*, 978–982.

The Langmuir model assumes that the maximum adsorption corresponds to a monolayer of adsorbate molecules on a homogeneous surface (i.e. with a constant energy). The equation in its linear form can be expressed as follows:

$$\frac{P}{V} = \frac{1}{K_L \cdot V_m} + \frac{P}{V_m}$$

where V and V_m are the equilibrium and maximum capacity of N_2 adsorption ($cm^3\ g^{-}1$), respectively, K_L is the Langmuir adsorption constant and P is the pressure at the equilibrium of the N_2 adsorbed gas. The value of V_m is extracted from the slope (1/Vm) of the linear plot of (P/V) vs. P.

Langmuir surface areas were calculated employing data points in the range of relative pressure (P/P°) from 0.0001 to 0.7

The equation of the BET theory is based on multilayer adsorption and can be written as follows:

$$\frac{\frac{P}{P^\circ}}{V(1-\frac{P}{P^\circ})} = \frac{1}{V_m \cdot C} + \frac{C-1}{V_m \cdot C} \cdot \frac{P}{P^\circ}$$

where V and V_m are the equilibrium and maximum capacity of N_2 adsorption ($cm^3\ g^{-1}$), P/P° is the relative pressure and C is the BET constant. *The value of V_m is extracted from the inverse of the (slope +intercept) of the linear plot of (P/P°)/(V(1- (P/P°))) vs. P/P°*

The BET specific surface areas were determined in the P/P^0 range from 0.001 to 0.05, identified by applying the four consistency criteria developed by Rouquerol et *al*. [2]: (i) the BET C constant should be positive; (ii) the function V(1- (P/P°)) should continuously increase with P/P°; (iii) the monolayer capacity (V_m) should correspond to a relative pressure P/P° included within the selected pressure; (iv) the calculated value for monolayer formation (1/(√C + 1)) should be approximately equal to P/P° at the monolayer formation (a tolerance of 20% has been accepted). In all cases, the four consistency criteria were satisfactorily fulfilled.

The t-plot method was used to estimate the amount of micropores based on the Halsey thickness equation. The total pore volumes were estimated from the adsorbed amounts at a relative pressure of ca. 0.95. Based on the N_2 adsorption data, a nonlocal density functional theory (NLDFT) model included in the commercial Tristar II 3020 V1.03 software was used for the calculation of pore size distributions (assuming cylindrical pore geometry).

NMR

^{1}H NMR spectra were recorded on a 300 MHz Bruker Avance III HD spectrometer using D_2O (99.92% isotopic purity, Eurisotop) as a solvent.

Field emission scanning electron microscopy (FE-SEM)

[2] J. Rouquerol, P. Llewellyn, F. Rouquerol, *Stud. Surf. Sci. Catal*. **2007**, 160, 40-56

Field emission scanning electron microscopy (FE-SEM) observations were performed to examine the morphology of the samples using a JEOL JSM-7800F LV field-emission microscope operating at 2 or 3 kV. Before imaging, samples were coated with a thin layer of chromium to reduce the accumulation of charges at high magnification.

Digestion experiments

Digestion experiments were carried out and monitored by ^{1}H NMR as follows: NH_2-UiO-66 (10 mg) and D_2O (600 µL) were introduced in a NMR tube. Sodium hydroxide (60 mg) was then added and the resultant solution was placed in an ultrasonic bath at room temperature for 10 s to provoke the MOF digestion. No signal relative to CD was detected.

The MOF structures were determined by liquid ^{1}H NMR measurements after sample digestion. From the relative peak area of aromatic H_2BDC-NH_2 protons and acetic acid methyl protons, UiO-66-NH_2 were formulated using the following equation:

$Zr_6O_4(OH)_4(H_2BDC\text{-}NH_2)_{(6\text{-}0.5X)}(\text{acetic acid})_X$

X = 6R/(1+0.5R), with R the NMR ratio of acetic acid to H_2BDC-NH_2.

Maleic acid was used as an internal reference (6.26 ppm) for the degradation under acidic conditions.

[3,4] The first step was to make two standard lines for the linker (2-aminoterephthalic acid) and the modulator (acetic acid) with various concentration ratios between the linker and the modulator with the reference (maleic acid). These lines are plotted considering the ratio of the concentrations as a function of the integrations of the respective peaks with each of the chemical species. Then, with a constant concentration of maleic acid, we proceed to the degradation in acidic environment of MOF UiO-66-NH_2 (mass of 2 mg for each sample in 120 µL of H_2SO_4 then removal of 50 µL of this solution, the tube was completed to 600 µL with DMSO-d6). Thanks to the ligand and modulator integration ratios with the reference, the ligand and modulator concentrations were determined in each of the digested samples, and the mass and mass fraction of each of the constituents of the MOF as well. The number of ligands and modulators per node Zr were given using the following formula:

$$\text{Number of ligand or modulator (i)} = w_i * M_{MOF} / M_i$$

w_i = weight fraction of ligand or modulator with respect to the total weight of MOF.

[3] R. Limvorapitux, H. Chen, M. L. Mendonca, M. Liu, R. Q. Snurr. S. T. Nguyen, *Catal. Sci. Technol.*, **2019**, *9*, 327-335.

[4] O. V. Gutov, M. González Hevia, E. C. Escudero-Adán, A. Shafir, Inorg. Chem. **2015**, *54*, 8396-8400.

Table S1. MOF formulas obtained from ^{1}H NMR at 25 °C in $CDCl_3$ (acidic digestion).

MOF	Formula	H_2BDC-NH_2	CH_3COOH	Number of free sites	H_2BDC-NH_2/Zr
Ideal Structure	$Zr_6O_4(OH)_4(C_6H_3NH_2(COO)_2)_6$	6	0	0	1.00
UiO-66-NH_2	$Zr_6O_4(OH)_{4.02}(C_6H_3NH_2(COO)_2)_{5.95}(CH_3COOH)_{0.08}$	5.95	0.08	0.02	0.99
UiO-66-NH_2_0.25αCD	$Zr_6O_4(OH)_{5.61}(C_6H_3NH_2(COO)_2)_{5.15}(CH_3COOH)_{0.08}$	5.15	0.09	1.61	0.86
UiO-66-NH_2_0.50αCD	$Zr_6O_4(OH)_{4.11}(C_6H_3NH_2(COO)_2)_{5.89}(CH_3COOH)_{0.11}$	5.89	0.11	0.11	0.98
UiO-66-NH_2_0.75αCD	$Zr_6O_4(OH)_{5.76}(C_6H_3NH_2(COO)_2)_{5.08}(CH_3COOH)_{0.08}$	5.08	0.08	1.76	0.85
UiO-66-NH_2_1αCD	$Zr_6O_4(OH)_{4.85}(C_6H_3NH_2(COO)_2)_{5.52}(CH_3COOH)_{0.11}$	5.52	0.11	0.85	0.92

Table S2. Textural characteristics of UiO-66-NH_2 (β-CD as co-modulator).

β-CD (equiv/ligand)	BET SSA (m^2/g)[a,b]	Langmuir SSA (m^2/g)[c]	S_{micro} (m^2/g)[d]	S_{micro} / BET SSA (%)	V_{micro} (cm^3/g)[e]	V_{total} (cm^3/g)[f]	V_{micro} / V_{total} (%)	Average pore diameter (Å)[g]
0	611 ± 6	706 ± 11	424	69.5	0.144	0.268	54.1	17.7
0.25	973 ± 26	1089 ± 29	716	73.6	0.250	0.402	62.3	16.5
0.50	1179 ± 27	1287 ± 18	862	73.1	0.300	0.458	65.4	15.5
0.75	939 ± 29	1048 ± 32	736	78.3	0.264	0.375	70.3	16.0
1	806 ± 17	889 ± 22	652	81.0	0.225	0.325	69.1	16.1

[a] Average of at least two experiments. [b] Specific surface area calculated from the Brunauer-Emmmet-Teller equation in the P/P° range from 0.001 to 0.05; [c] Specific surface area calculated from the Langmuir equation in the P/P° range from 0.001 to 0.70; [d] Micropore surface area determined by the t-plot method; [e] Micropore volume determined by the t-plot method; [f] Total pore volume estimated at P/P° = 0.95; [g] Average pore based on $4 \times V_{total}$/ BET SSA

Table S3. Textural characteristics of UiO-66-NH_2 (γ-CD as co-modulator).

γ-CD (equiv/ligand)	BET SSA (m^2/g)[a,b]	Langmuir SSA (m^2/g)[c]	S_{micro} (m^2/g)[d]	S_{micro} / BET SSA (%)	V_{micro} (cm^3/g)[e]	V_{total} (cm^3/g)[f]	V_{micro} / V_{total} (%)	Average pore diameter (Å)[g]
0	611 ± 6	706 ± 11	424	69.5	0.144	0.268	54.1	17.7
0.25	377 ± 3	444 ± 22	268	71.3	0.107	0.187	59.4	19.8
0.50	307 ± 11	358 ± 41	229	74.6	0.080	0.153	52.3	20.1
0.75	149 ± 6	166 ± 6	84	65.1	0.028	0.087	32.0	27.0
1	39 ± 4	59 ± 2	23	55.8	0.006	0.035	16.6	34.2

[a] Average of at least two experiments. [b] Specific surface area calculated from the Brunauer-Emmmet-Teller equation in the P/P° range from 0.001 to 0.05; [c] Specific surface area calculated from the Langmuir equation in the P/P° range from 0.001 to 0.70; [d] Micropore surface area determined by the t-plot method; [e] Micropore volume determined by the t-plot method; [f] Total pore volume estimated at P/P° = 0.95; [g] Average pore based on $4 \times V_{total}$/ BET SSA.

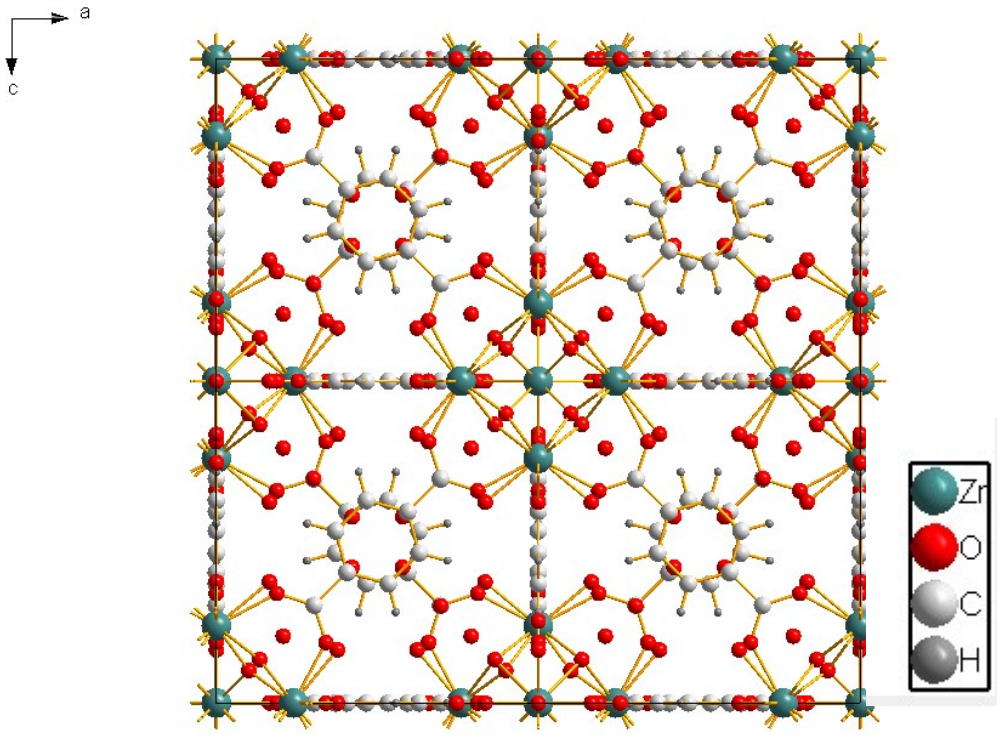

Figure S1. Structural representation of the UiO-66-NH_2 arrangement showing Face-Centered-Cubic structure with *Fm*-3*m* space group. NH_2 groups are omitted for clarity, due to disordered configuration.

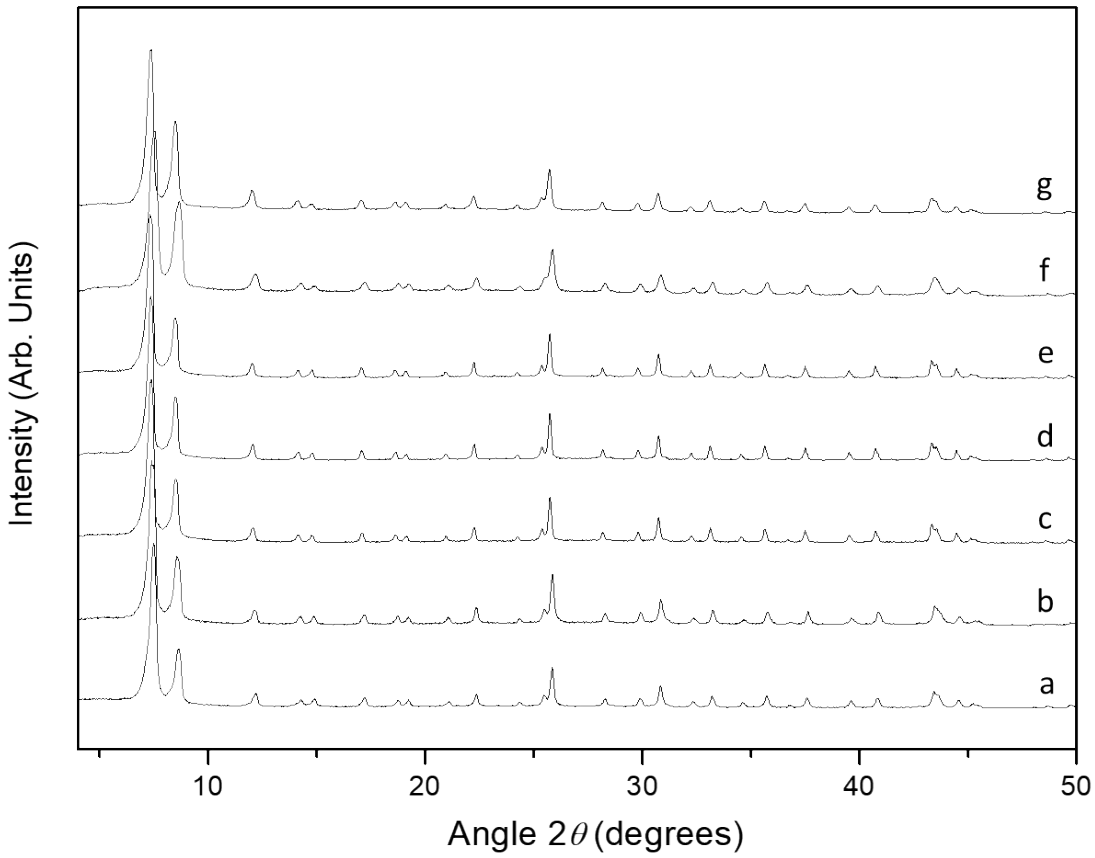

Figure S2. XRD patterns of UiO-66-NH_2 derived from mixtures containing α-CD in various proportions. n = number of equivalents of α-CD with respect to the ligand. a) n=0, b) n = 0.05, c) n=0.10, d) n=0.25, e) n=0.5, f) n=0.75, g) n=1, h) n=1.5, and i) n=2.

For the XRD patterns of UiO-66-NH_2 derived from mixtures containing α-CD, a unique phase is observed and the more intense Bragg peaks are centered at 2θ=7.38, 8.52, 17.10, 19.13, 22.27, 25.76, 29.83, 33.17, 35.69, 40.80, 43.63 and 49.72° indexed with (111), (002), (004), (024), (115), (006), (444), (355), (446), (466), (068) and (088) reflections, respectively.

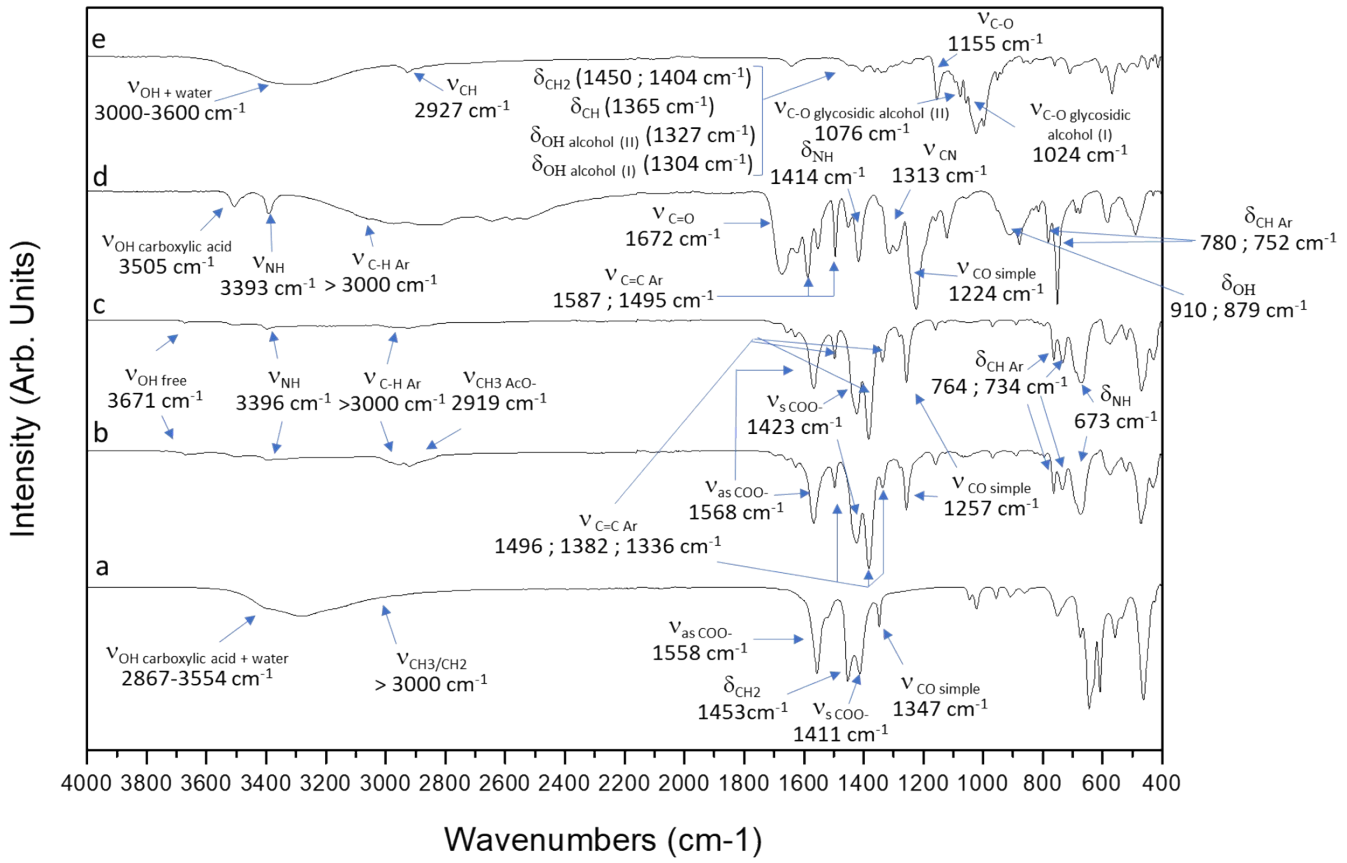

Figure S3. FTIR spectra of $Zr_6O_4(OH)_4(CH_3COO)_{12}$ (a), UiO-66-NH_2 (b), UiO-66-NH_2 synthesized with 1 equivalent α-CD with respect to the ligand (c), 2-aminoterephthalic acid (d) and α-CD (e).

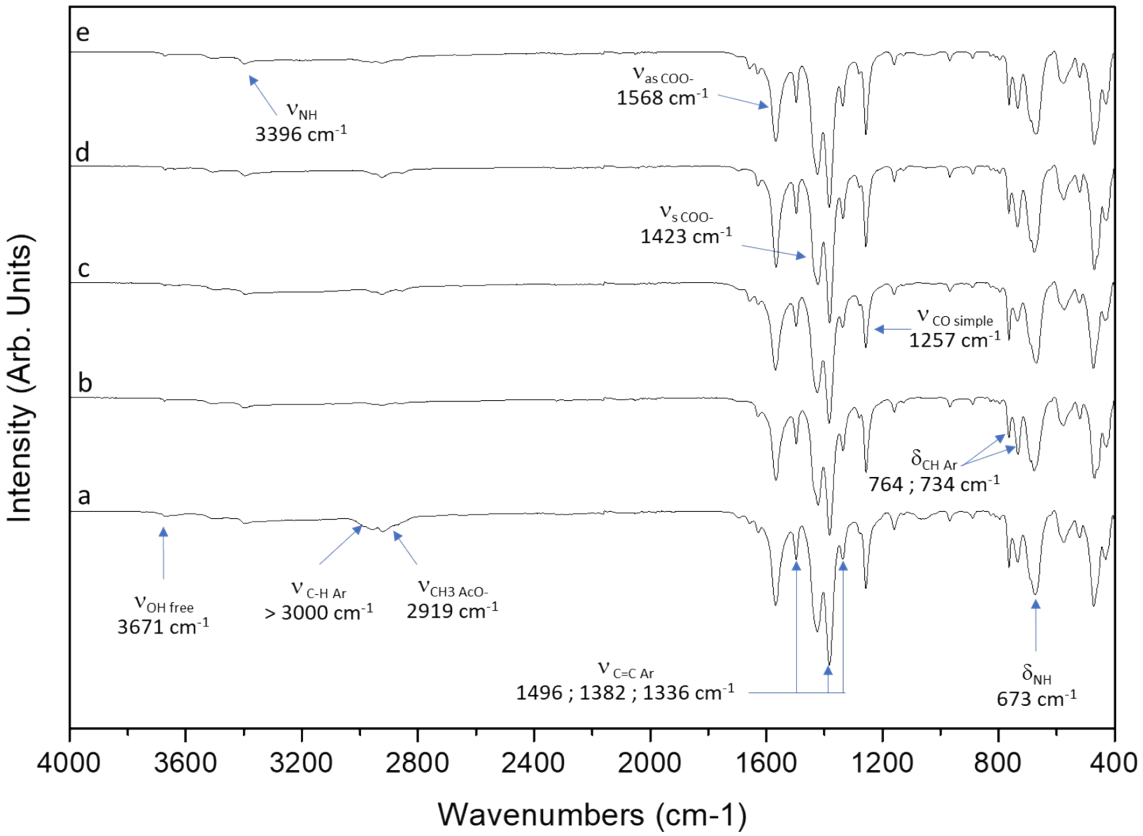

Figure S4. FTIR spectra of UiO-66-NH_2 synthesized with α-CD/ligand molar ratios of 0 (a), 0.25 (b), 0.5 (c), 0.75 (d), and 1 (e).

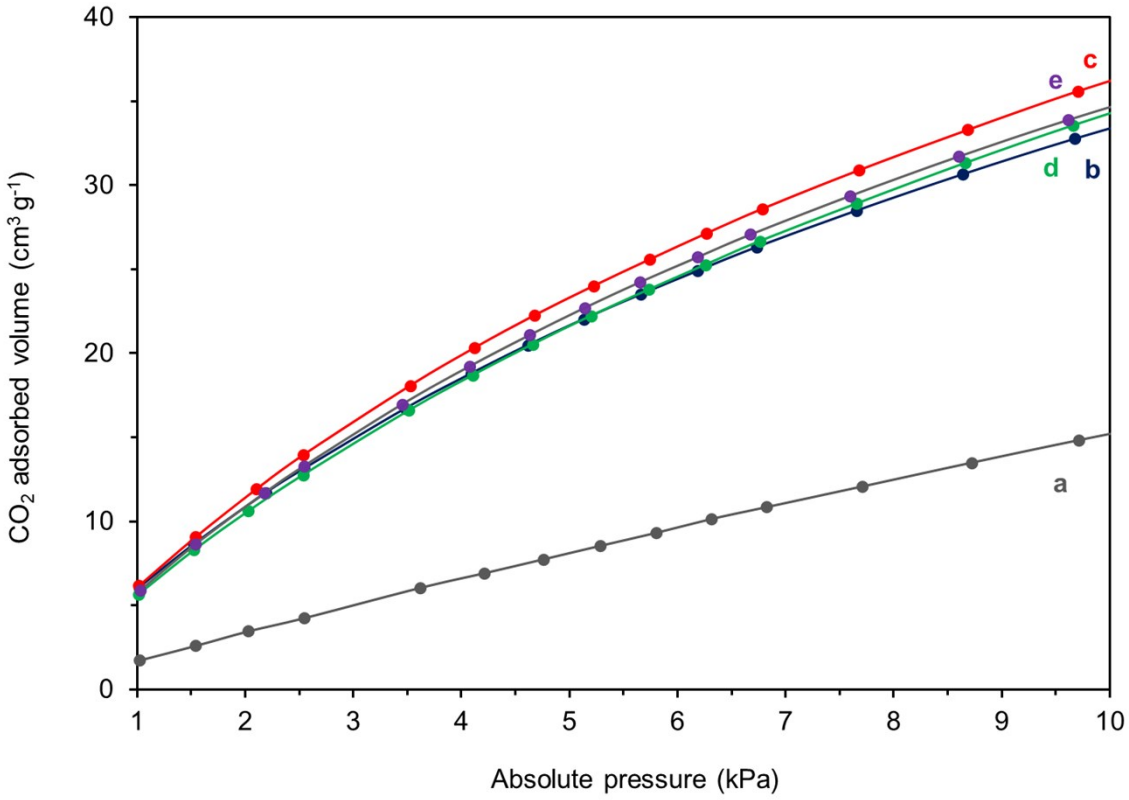

Figure S5. CO_2 sorption isotherms collected at 0°C (273 K) of UiO-66-NH_2 synthesized with ground H_2BDCNH_2 and various amounts of α-CD: 0 equiv/Zr (a, grey), 0.25 equiv/Zr (b, blue), 0.5 equiv/Zr (c, red), 0.75 equiv/Zr (d, green), and 1 equiv/Zr (e, violet).

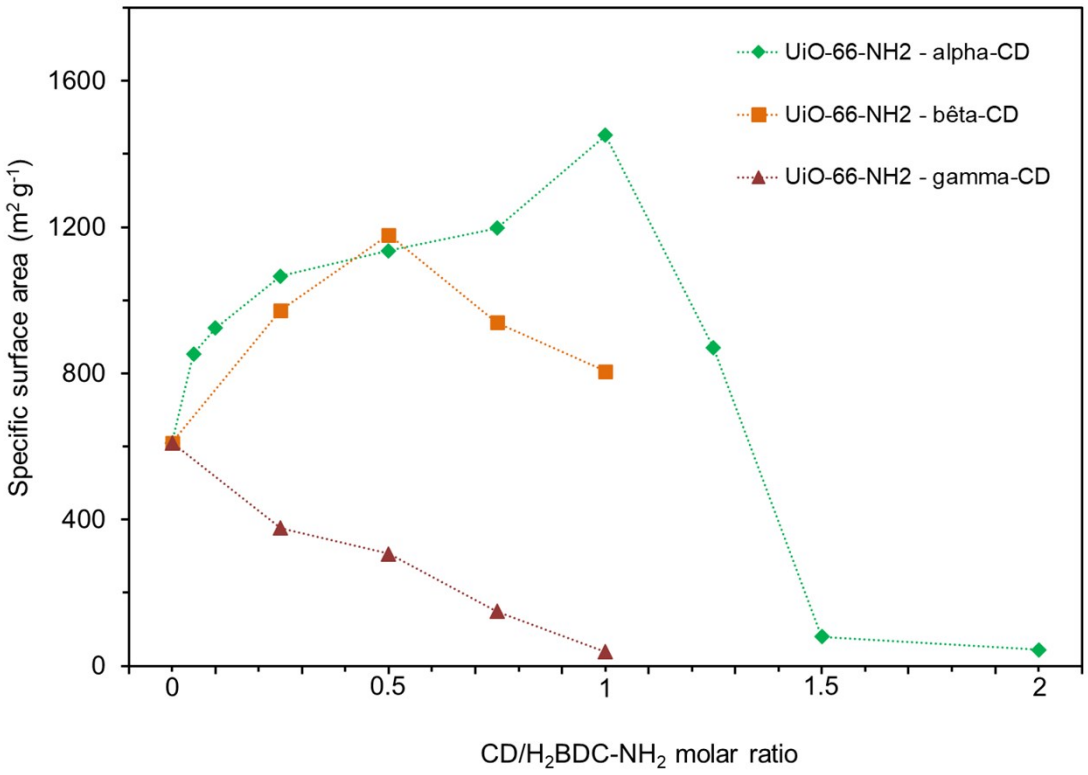

Figure S6. Variation of the specific surface area (SSA) measured by BET with the quantity of CD. α-CD (red); β-CD (black); γ-CD (blue).

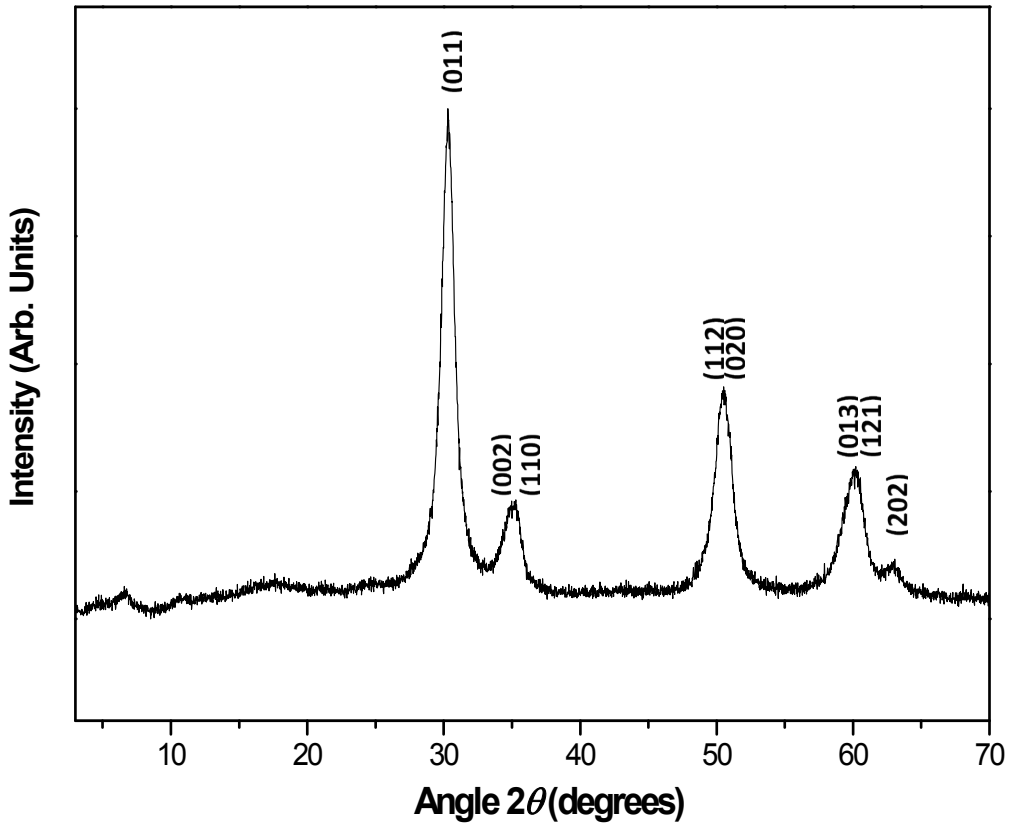

Figure S7. XRD pattern of UiO-66-NH2 after a thermal treatment at 550°C under air flow. The XRD pattern clearly shows the stabilization of the tetragonal phase of ZrO_2 as evidenced by the set of characteristic Bragg reflections (JCPDS card no. 17-0923).

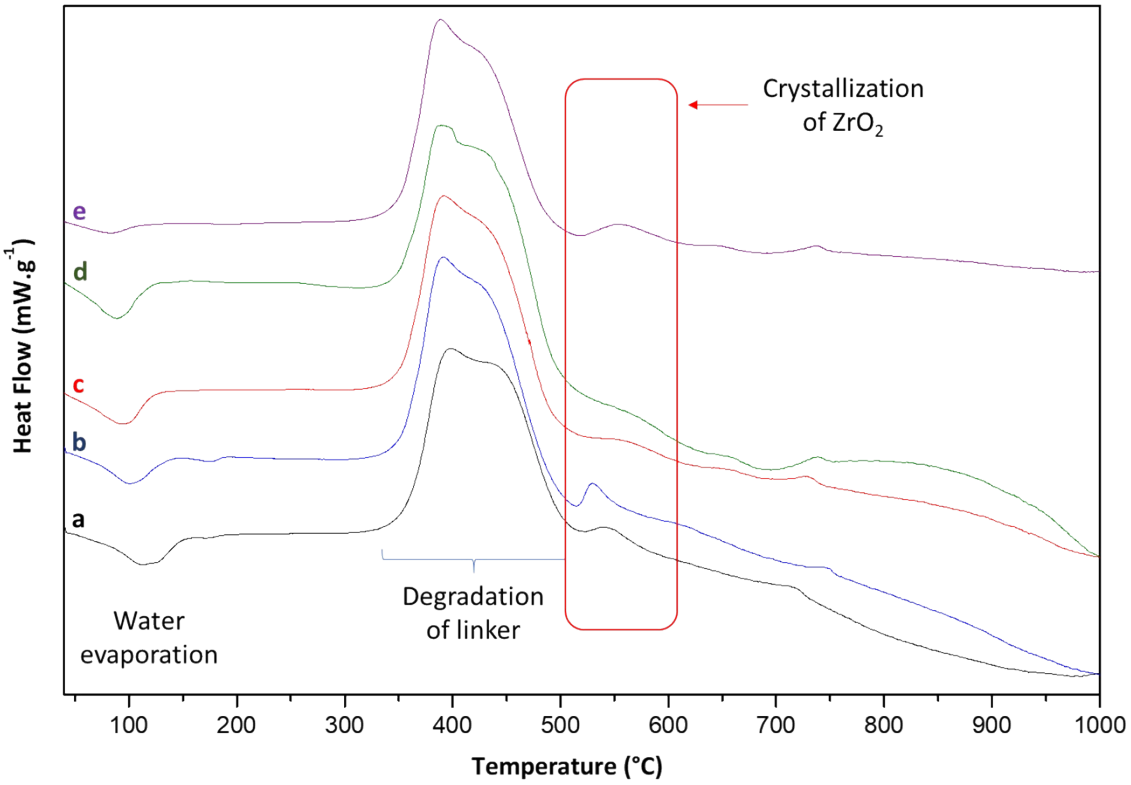

Figure S8. Variation of heat flow with the temperature measured by DSC. 0 equiv. α-CD/H_2BDC-NH_2 (a), 0.25 equiv. (b), 0.5 equiv (c), 0.75 equiv. (d), and 1 equiv. (e).

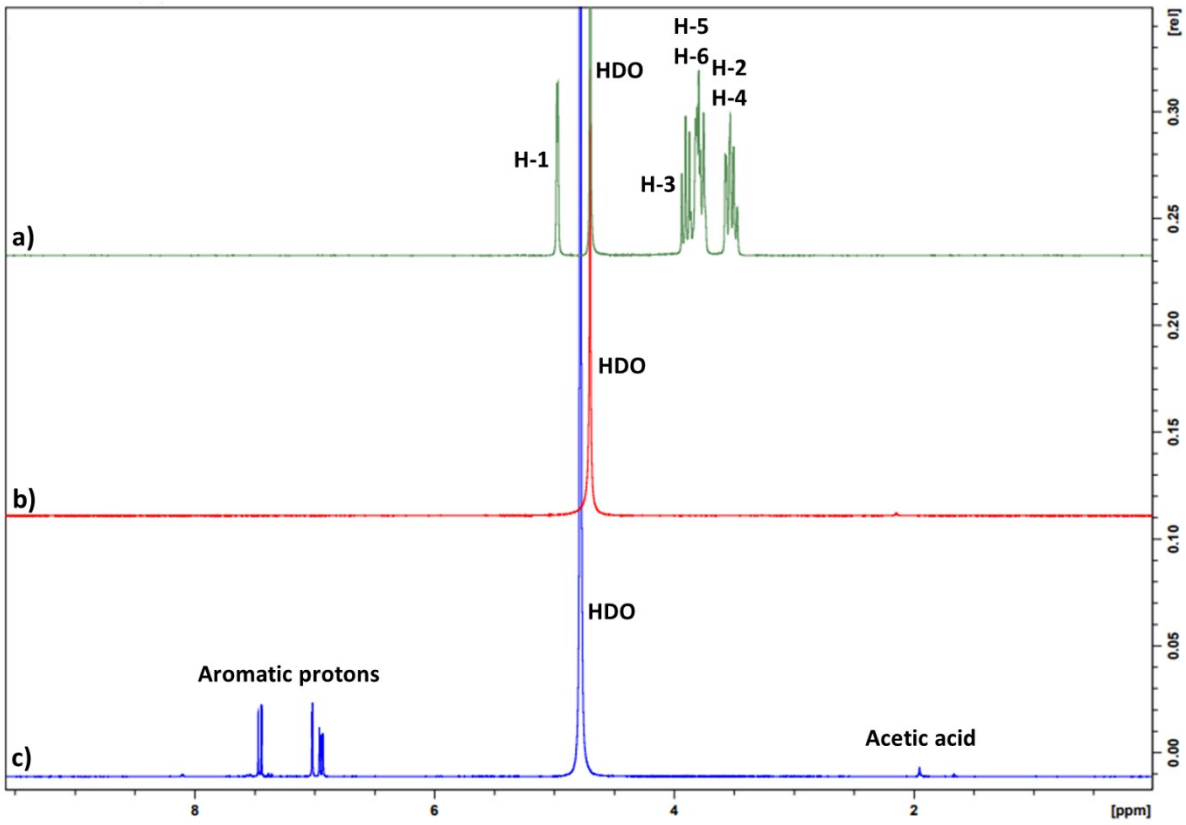

Figure S9. ^{1}H NMR spectra in D_2O at 25 °C of a) α-CD, b) UiO-66-NH_2 synthesized with α-CD as co-modulator, and c) compounds resulting from digestion by NaOH of UiO-66-NH_2 synthesized with α-CD as co-modulator.

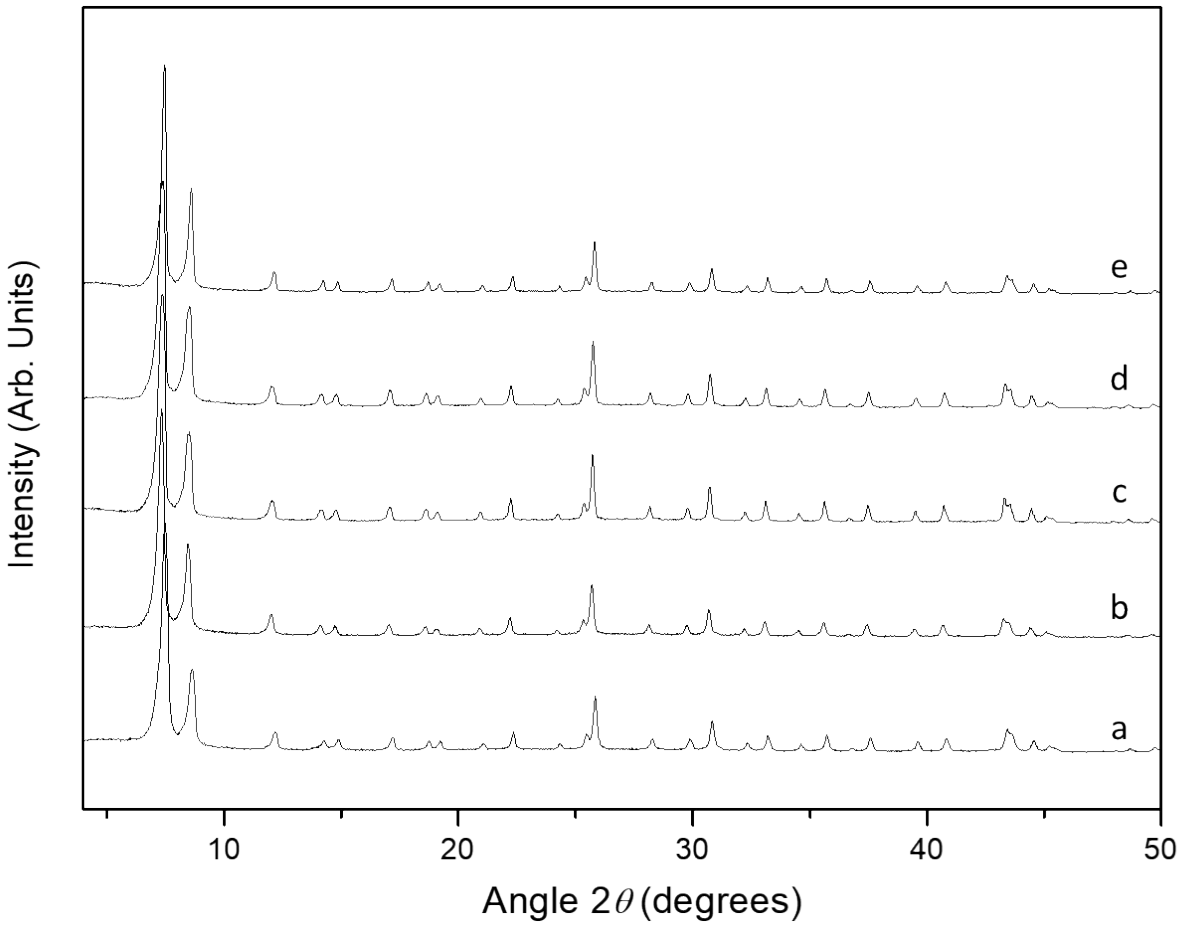

Figure S10. XRD patterns of UiO-66-NH_2 derived from mixtures containing β-CD in various proportions. n = number of equivalents of β-CD with respect to the H_2BDC-NH_2 ligand. a) n=0, b) n=0.25, c) n=0.5, d) n=0.75, and e) n=1.

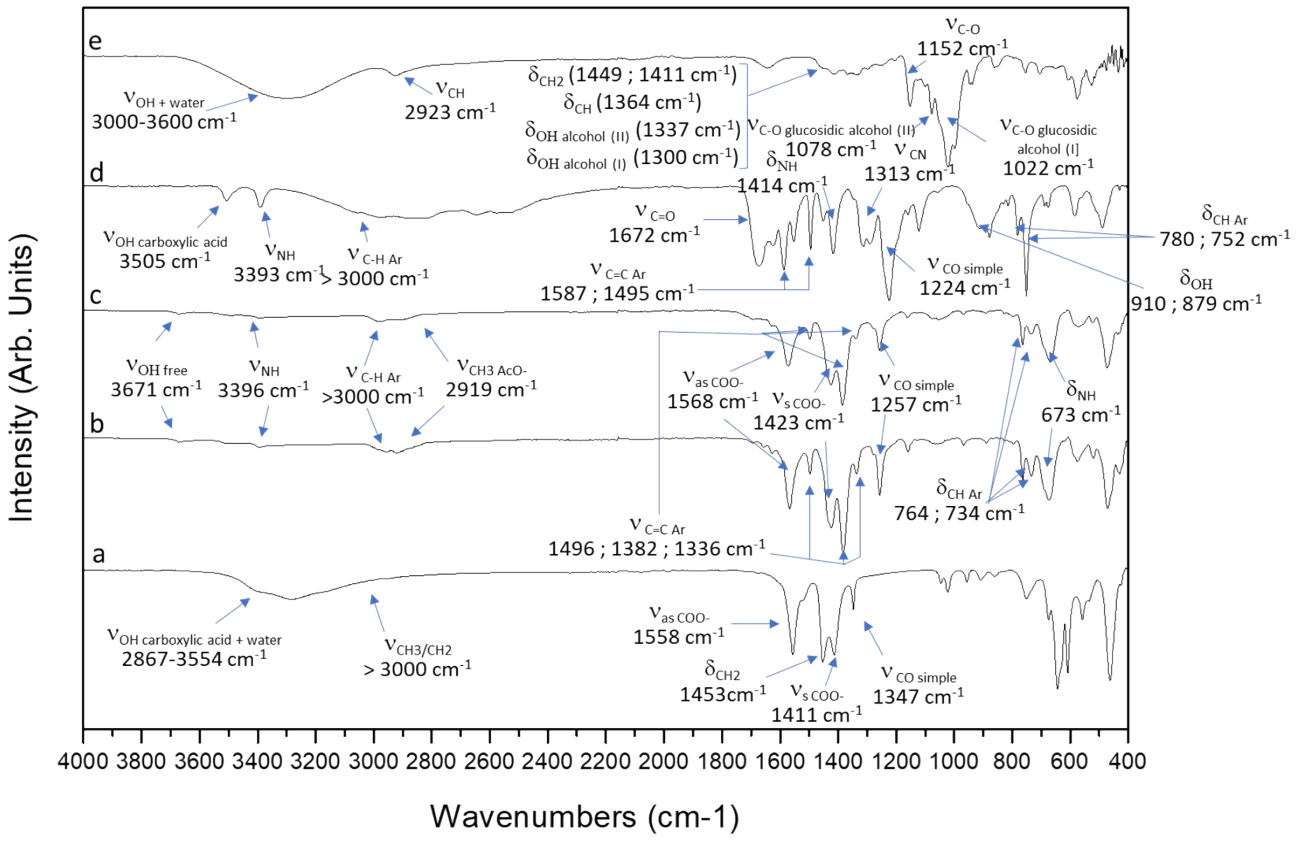

Figure S11. FTIR spectra of $Zr_6O_4(OH)_4(CH_3COO)_{12}$ (a), UiO-66-NH_2 (b), UiO-66-NH_2 synthesized with 1 equivalent β-CD with respect to the ligand (c), 2-aminoterephthalic acid (d) and β-CD (e).

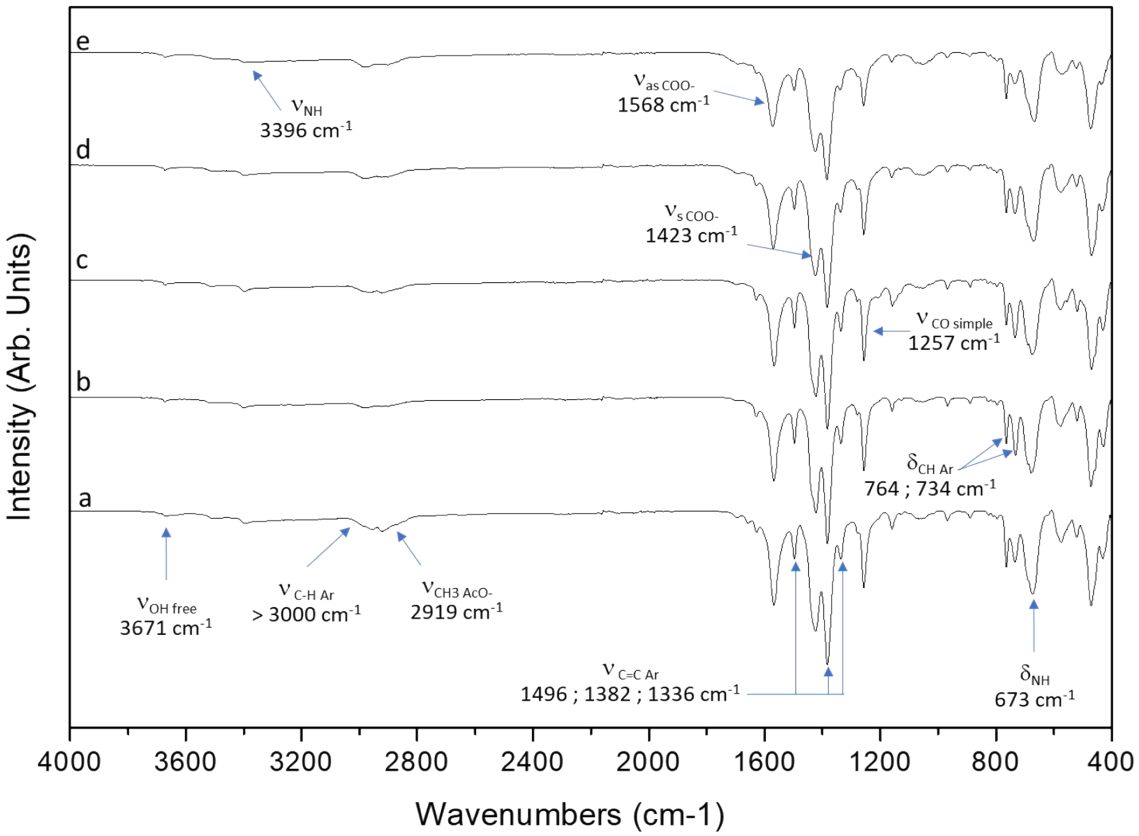

Figure S12. FTIR spectra of UiO-66-NH_2 synthesized with β-CD/ligand molar ratios of 0 (a), 0.25 (b), 0.5 (c), 0.75 (d), and 1 (e).

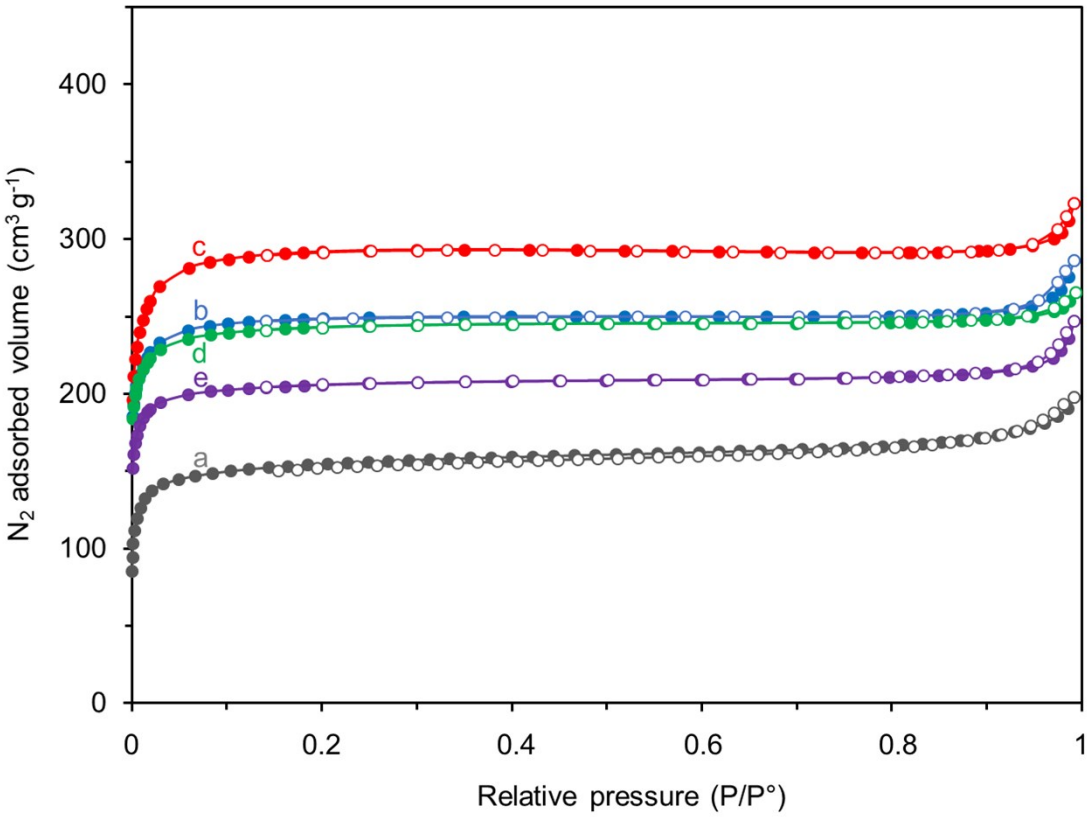

Figure S13. N_2 sorption isotherms collected at 77K of UiO-66-NH_2 synthesized using various amounts of ground β-CD with respect to ground H_2BDC-NH_2 [Adsorption (filled circles) and desorption (open circles)]. 0 equiv. α-CD/ H_2BDC-NH_2 (a, grey), 0.25 equiv. (b, blue), 0.5 equiv. (c, red), 0.75 equiv. (d, green), and 1 equiv. (e, violet).

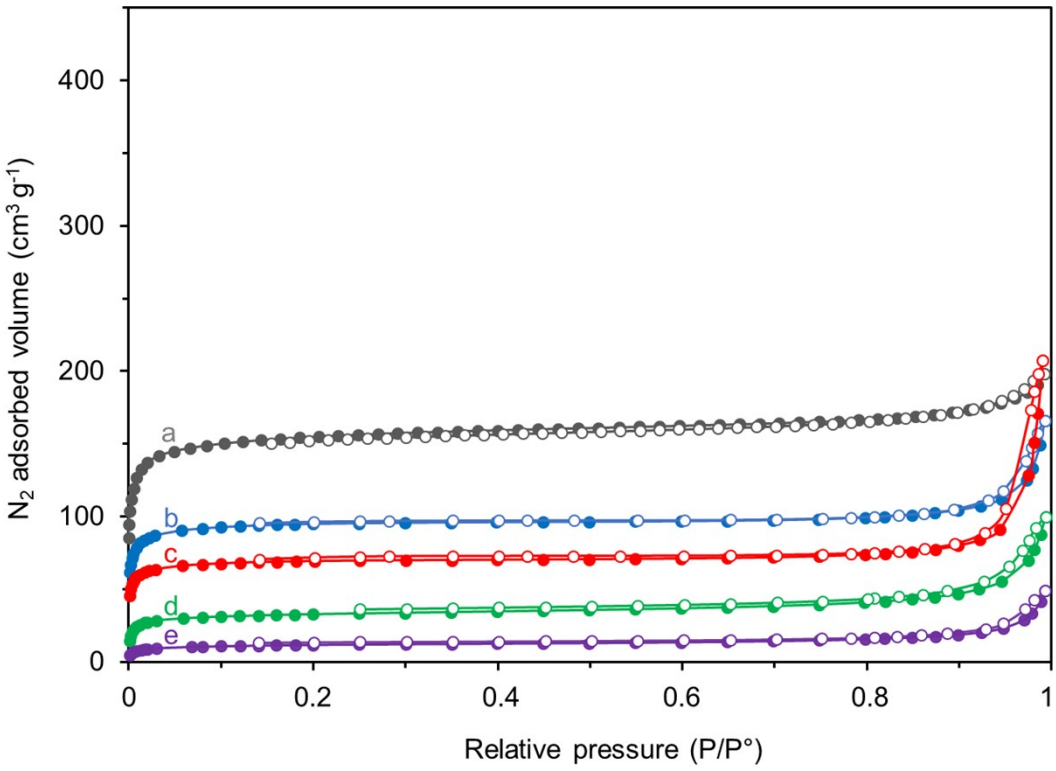

Figure S14. N_2 sorption isotherms collected at 77K of UiO-66-NH_2 synthesized using various amounts of ground γ-CD with respect to ground H_2BDC-NH_2 [Adsorption (filled circles) and desorption (open circles)]. 0 equiv. α-CD/ H_2BDC-NH_2 (a, grey), 0.25 equiv. (b, blue), 0.5 equiv. (c, red), 0.75 equiv. (d, green), and 1 equiv. (e, violet).

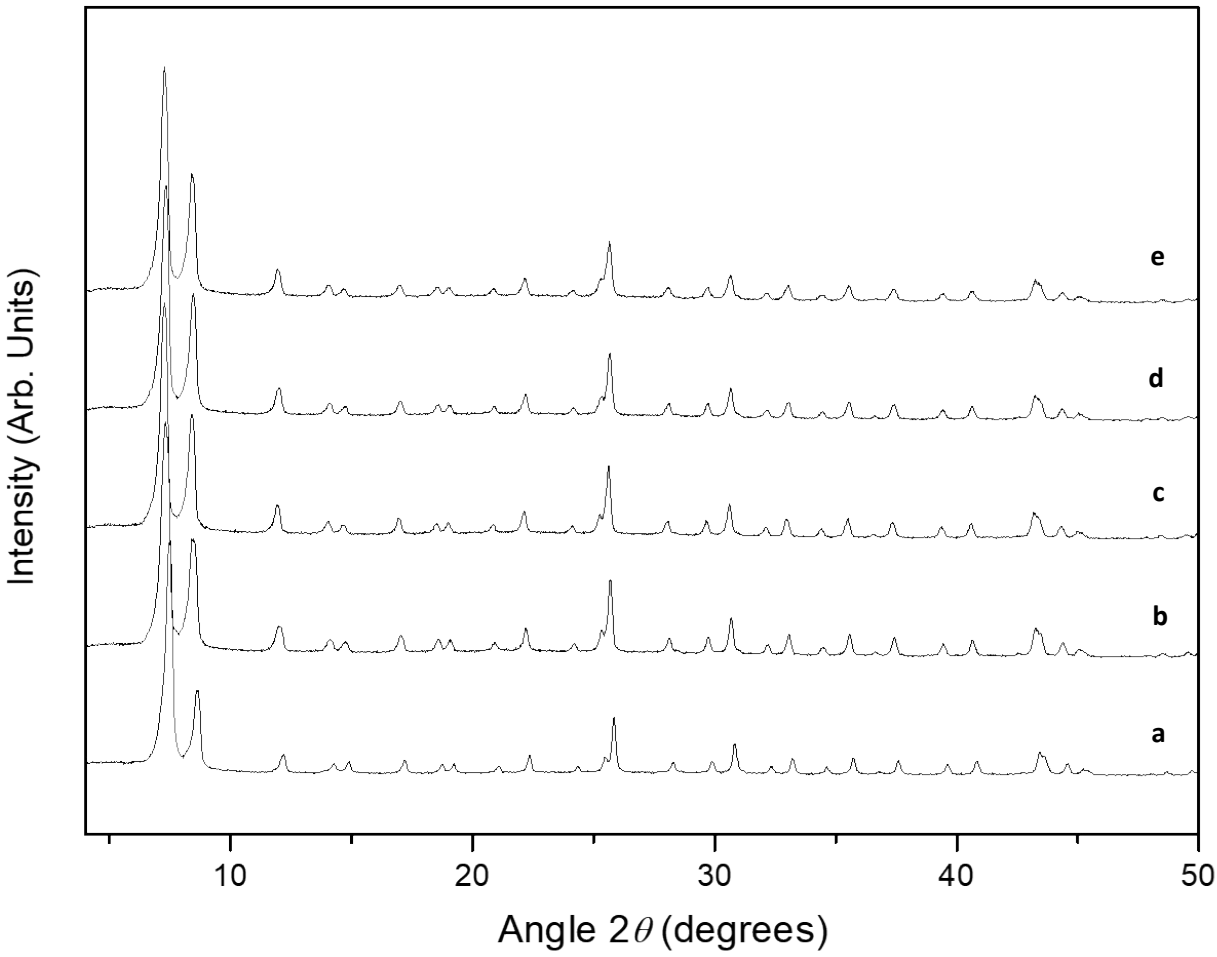

Figure S15. XRD patterns of UiO-66-NH_2 derived from mixtures containing γ-CD in various proportions. n = number of equivalents of γ-CD with respect to the H_2BDC-NH_2 ligand. a) n=0, b) n=0.25, c) n=0.5, d) n=0.75, and e) n=1.

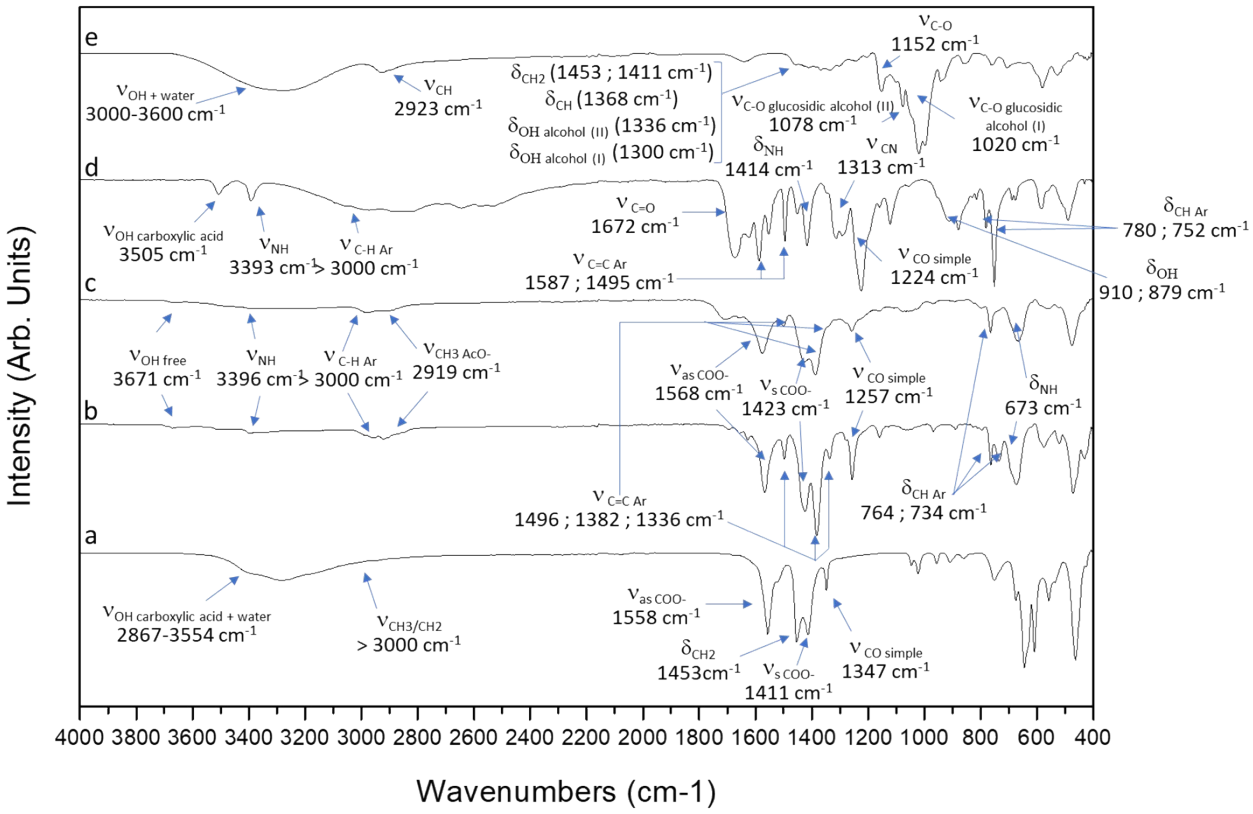

Figure S16. FTIR spectra of $Zr_6O_4(OH)_4(CH_3COO)_{12}$ (a), NH_2-UiO-66 (b), UiO-66-NH_2 synthesized with 1 equivalent γ-CD with respect to the ligand (c), 2-aminoterephthalic acid (d) and γ-CD (e).

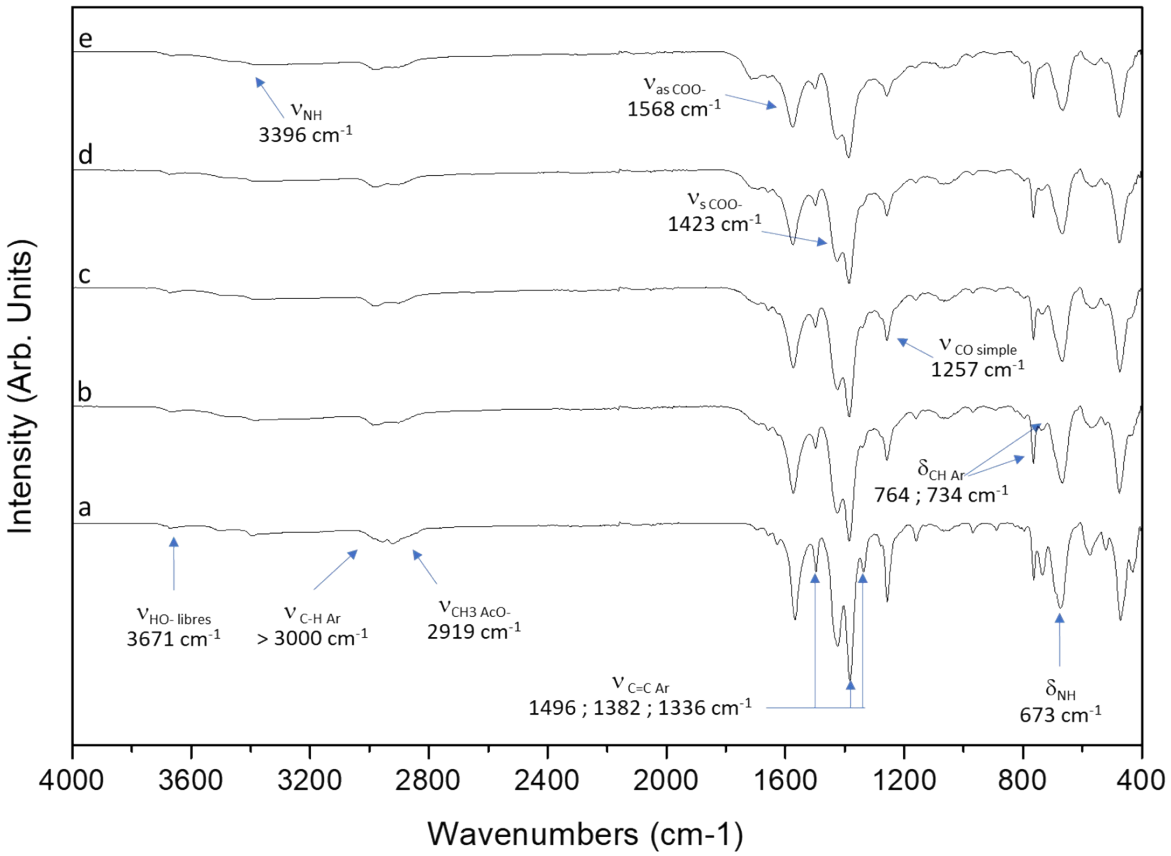

Figure S17. FTIR spectra of UiO-66-NH_2 synthesized with γ-CD/ligand molar ratios of 0 (a), 0.25 (b), 0.5 (c), 0.75 (d), and 1 (e).

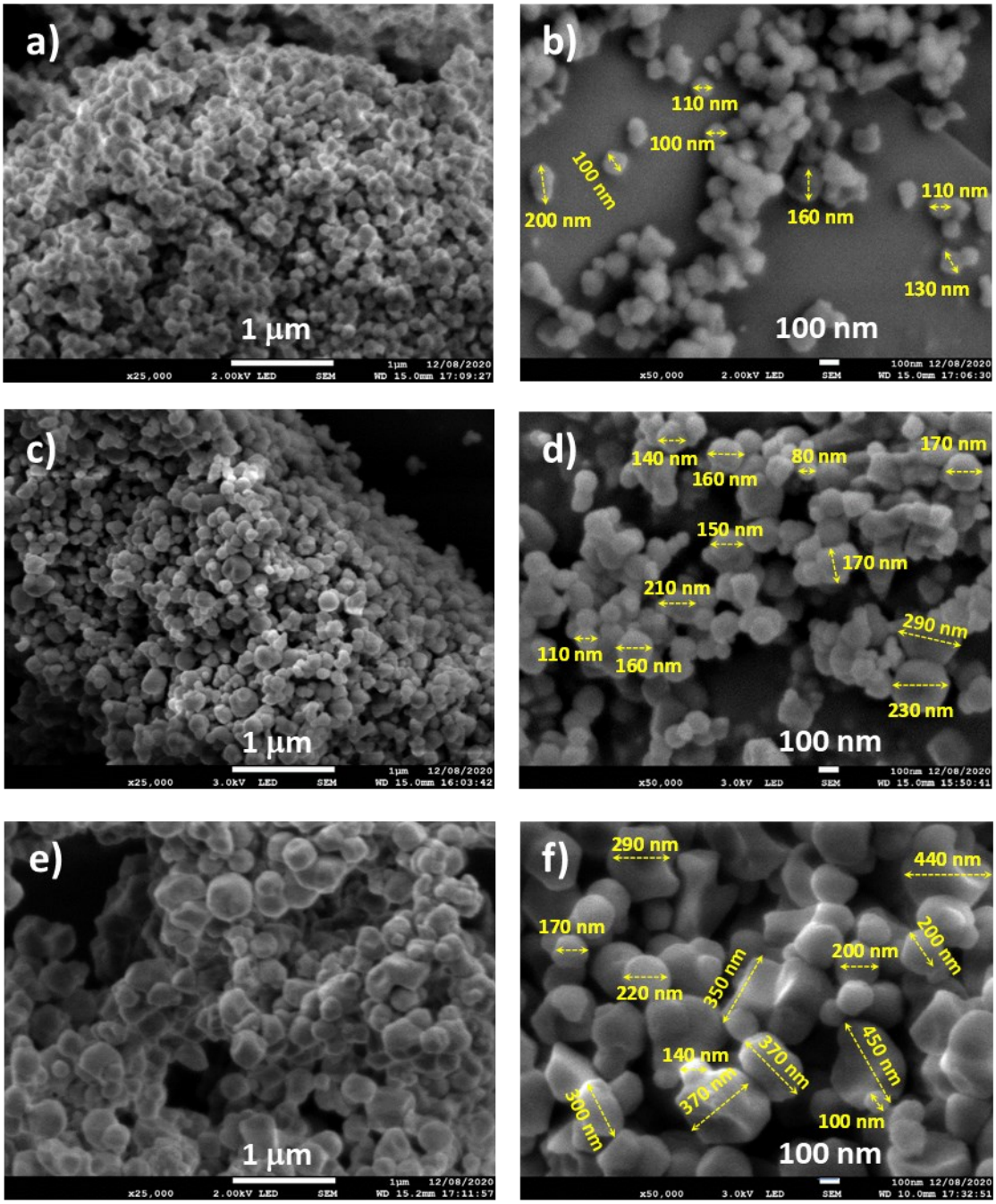

Figure S18. Transmission Electron Micrographs of UiO-66-NH_2 synthesized without α-CD (a and b), with 0.5 equiv. α-CD with respect to the linker (c and d), and with 0.5 molar equiv. of β-CD with respect to the linker (e and f) with dimensions of crystallites. Magnification: 25,000x (left column) and 50,000x (right column).

a)

Dispersion	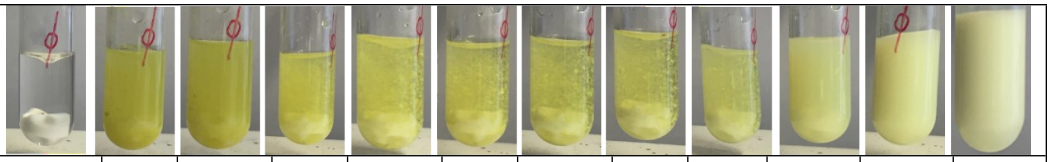											
Time (s)	[a]	0	30	60	90	120	150	180	210	240	270	300

[a] before addition of ground H_2-BDCNH$_2$.

b)

Dispersion	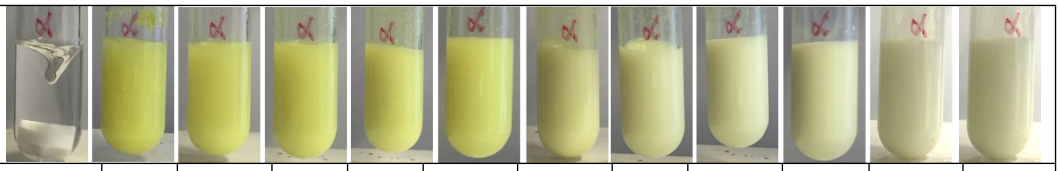											
Time (s)	[a]	0	30	60	90	120	150	180	210	240	270	300

[a] before addition of a ground mixture of H_2-BDCNH$_2$ and αCD.

c)

Dispersion	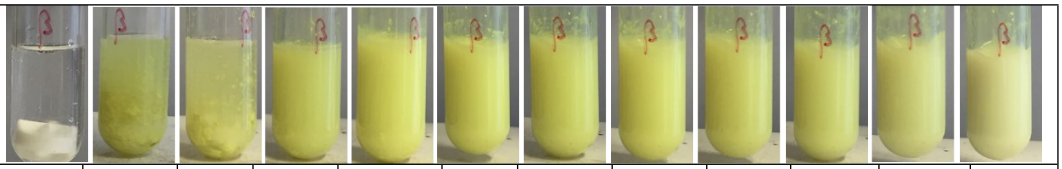											
Time (s)	[a]	0	30	60	90	120	150	180	210	240	270	300

[a] before addition of a ground mixture H_2-BDCNH$_2$ and βCD.

d)

Dispersion	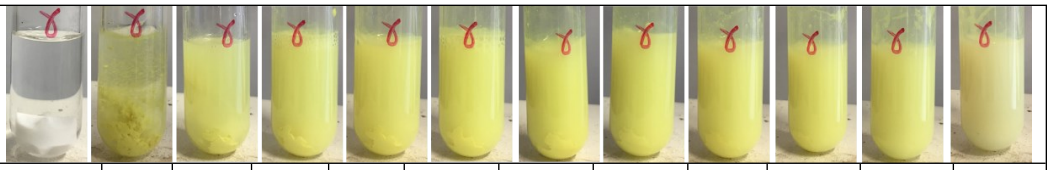											
Time (s)	[a]	0	30	60	90	120	150	180	210	240	270	300

[a] before addition of a ground mixture of H_2-BDCNH$_2$ and γCD.

Figure S19. Dispersion with time of aqueous solutions containing $ZrOCl_2.8H_2O$ (322.25 mg, 1 mmol), 2-aminoterephthalic acid (181.15 mg, 1 mmol) in a mixture of water/acetic acid (5 mL/5 mL) without α-CD (a), and in the presence of α-CD (486 mg, 0.5 mmol) (b), β-CD (568 mg, 0.5 mmol) (c), and γ-CD (649 mg, 0.5mmol) (d).

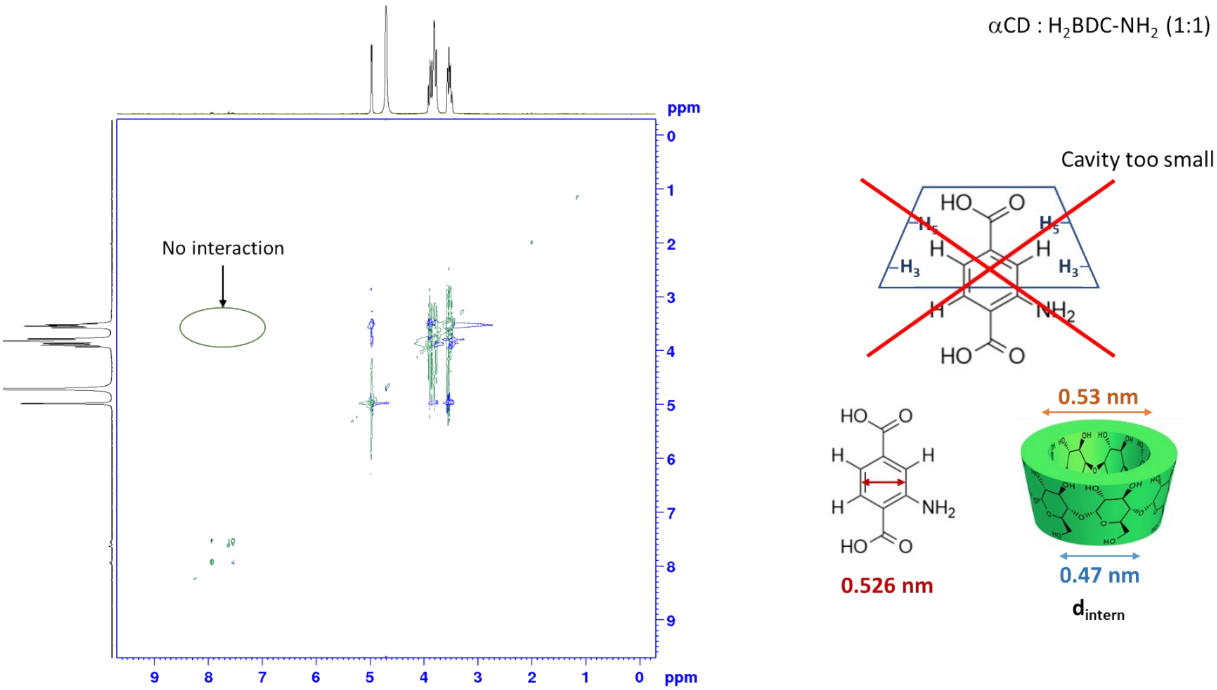

Figure S20. 2D T-ROESY NMR spectrum in D_2O at 25 °C of a 1/1 mixture of α-CD and *H*$_2$BDC-NH_2 (3 mM).

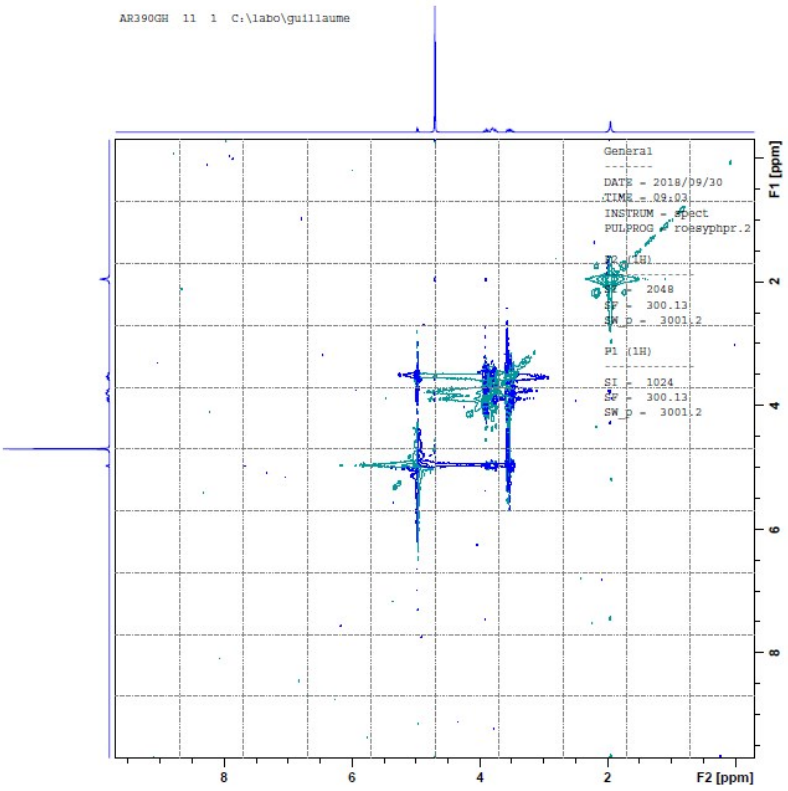

Figure S21. 2D T-ROESY NMR spectrum in D_2O at 25 °C of a 1/1 mixture of α-CD and Zr-oxyacetate clusters (3 mM).

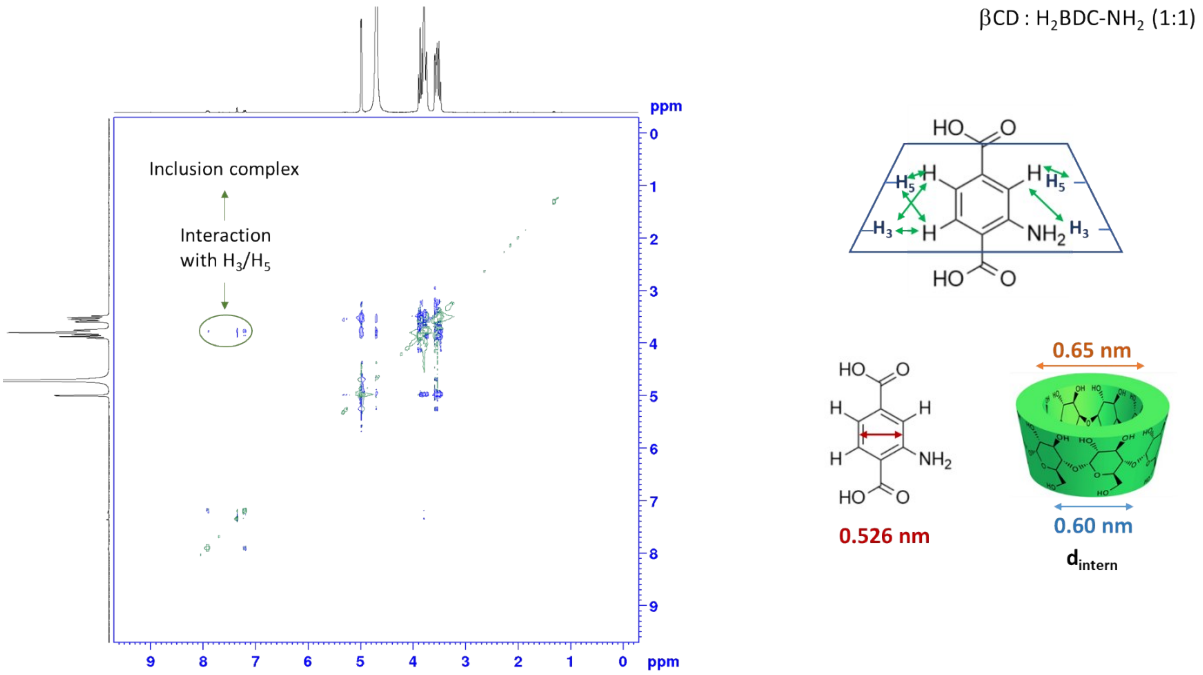

Figure S22. 2D T-ROESY NMR spectrum in D_2O at 25 °C of a 1/1 mixture of β-CD and *H*$_2$BDCNH$_2$ (3 mM).

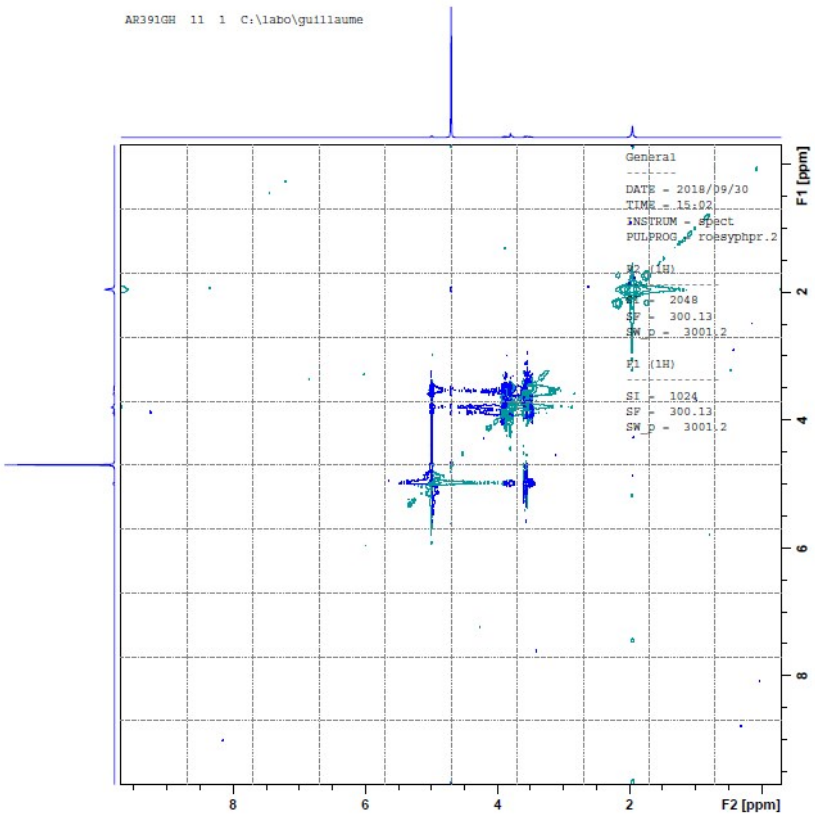

Figure S23. 2D T-ROESY NMR spectrum in D_2O at 25 °C of a 1/1 mixture of β-CD and Zr-oxyacetate clusters (3 mM).

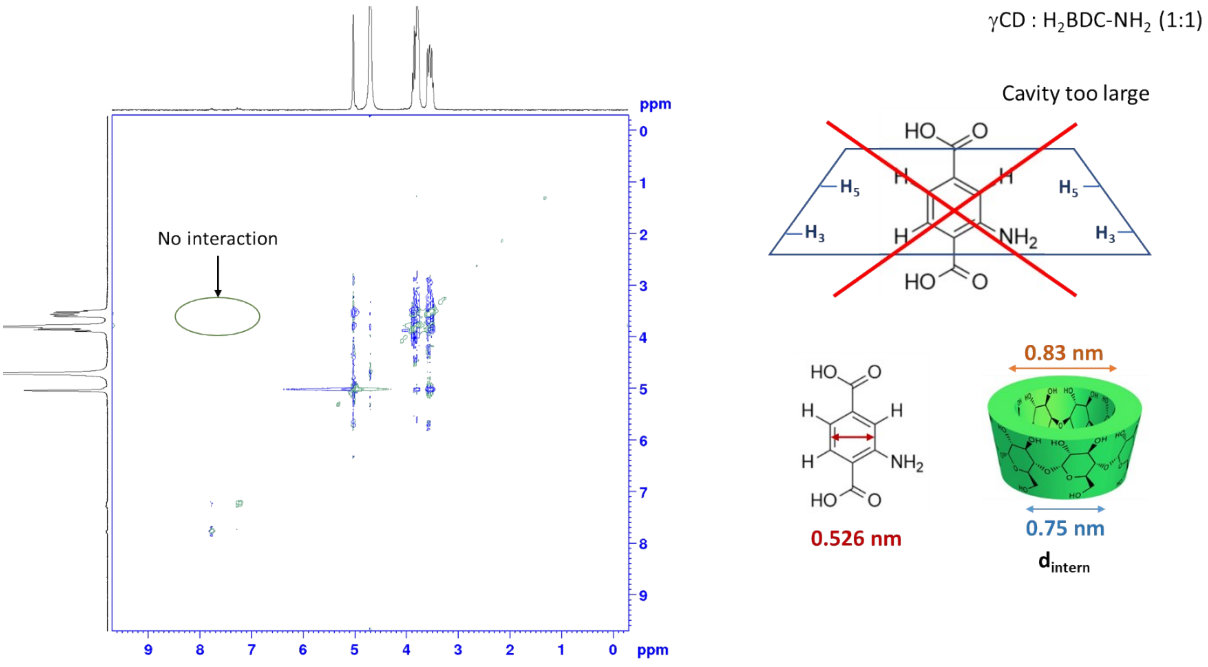

Figure S24. 2D T-ROESY NMR spectrum in D_2O at 25 °C of a 1/1 mixture of γ-CD and *H*$_2$BDCNH$_2$ (3 mM).

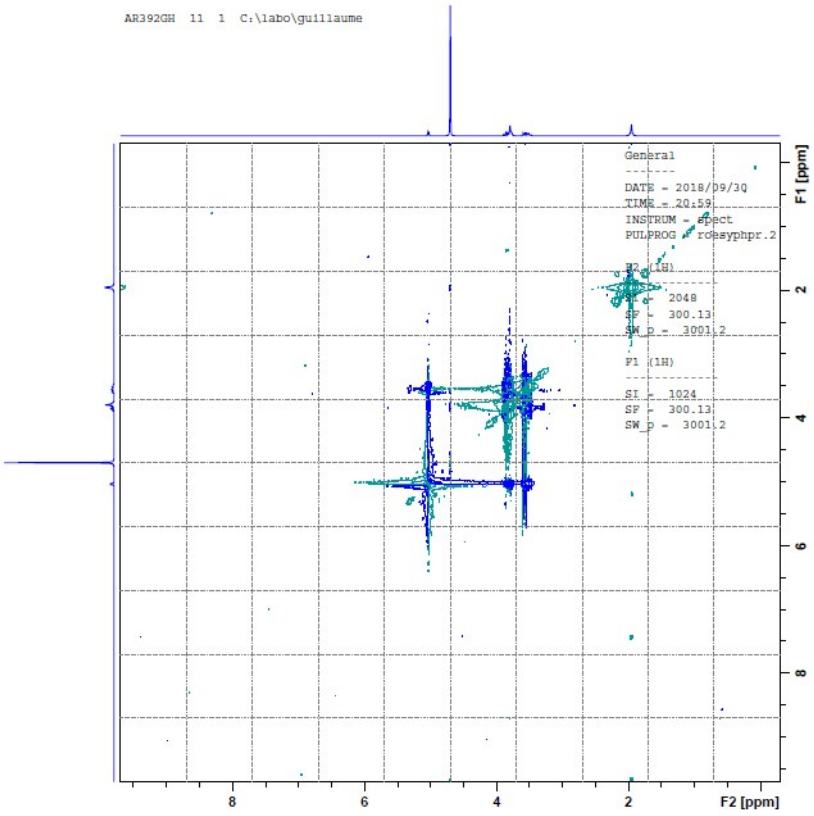

Figure S25. 2D T-ROESY NMR spectrum in D_2O at 25 °C of a 1/1 mixture of γ-CD and and Zr-oxyacetate clusters (3 mM).